The decisive role of Cu^{I}-framework O binding in oxidation half cycle of selective catalytic reduction

Yiyun Liu[1], Jasper Berry-Gair[2], Zhipeng Wang[1], Liqun Kang[1], Bolun Wang[1], Xuze Guan[1], Sushila Marlow[1], Junrun Feng[1], Loredana Mantarosie[3], David Thompsett[3], Misbah Sarwar[3], Maria Pia Ruggeri[3], Shusaku Hayama[4], Furio Cora[2], Feng Ryan Wang[1]**

[1] *Department of Chemical Engineering, University College London, Roberts Building, Torrington Place, London, WC1E 7JE, United Kingdom*

[2] *Department of Chemistry, University College London, 20 Gordon Street, London, WC1H 0AJ, United Kingdom*

[3] *Johnson Matthey Technology Centre, Blounts Court Road, Sonning Common, Reading RG4 9NH, United Kingdom*

[4] *Diamond Light Source, Harwell Science & Innovation Campus, Didcot, OX11 0DE, United Kingdom*

KEYWORDS

SCR mechanism, $Cu^{I}(NH_3)_xO_{fw}$, HERFD-XANES, VtC-XES, side on O_2

ABSTRACT

Cu-exchanged zeolite is an efficient catalyst to remove harmful nitrogen oxides from diesel exhaust gas through the selective catalytic reduction (SCR) reaction. The SCR performance is structure dependent, in which a Cu with one adjacent framework Al (1AlCu) has lower activation energy in oxidative half-cycle than Cu with two adjacent framework Al (2AlCu). Using a combination of *operando* X-ray absorption spectroscopy, valence to core - X-ray emission spectroscopy and density functional theory calculations, here we showed that 1AlCu

proceeds with nitrate mechanism, in which side-on coordination of O_2 at a $Cu^{I}(NH_3)_xO_{fw}$ (fw = framework) is the rate-limiting step in the oxidation half-cycle. As a result, the $Cu^{I}(NH_3)_xO_{fw}$ at 1AlCu can easily yield a transient $Cu^{II}NO_x$ intermediate upon breaking of Cu-O_{fw} after interaction with NO. In the meantime, 2AlCu has high barriers for Cu-O_{fw} bond breaking and proceeds with dimer mechanism. Our results show the coexisting of both dimer and nitrate mechanism, in particular at high Cu loadings, in which controlling the strength of the Cu-O_{fw} coordination is key for the O-O split in the nitrate pathway.

1. Introduction

Nitrogen oxides (NO_x) are one of the major pollutants in the exhaust gas of power plants and vehicles, threatening public health and the environment. NH_3-assisted selective catalytic reduction (SCR) of NO_x on Cu-exchanged chabazite (Cu-CHA) zeolites have high NO_x conversion in a wide temperature range and good hydrothermal stability[1-4]. Driven by the need to improve the low temperature de-NO_x activity to meet tightening legislation on emission control, it is important to study and understand the SCR mechanism. The mechanism contains a reduction cycle from Cu^{II} to Cu^{I} and then an oxidative cycle back to Cu^{II}. In the reductive cycle, it is generally agreed that Cu^{II} is reduced by NO and NH_3 together through the formation of NH_4NO_2[3, 5, 6] and/or H_2NNO[7-9] intermediates. However, the mechanism of the oxidative half cycle at low temperature remains debated. One proposed mechanism uses the formation of transient $[Cu^{I}(NH_3)_2]^{+}$-O_2-$[Cu^{I}(NH_3)_2]^{+}$ intermediates from two mobile Cu^{I} ions to explain the quadratic dependent relationship between SCR rate and Cu concentration at low Cu density[6, 10]. For high Cu density, a variety of Cu species are formed, which means a combination of different reaction mechanism will occur as shown in the increase of activation energy. One mechanism is

proposed to emphasize the importance of both NO and O_2 in the oxidation of Cu^I, forming intermediate nitrate/nitrite species ($CuNO_x$)[8] due to the presence of different Cu active species.

The oxidation half cycle is affected by the local coordination environment of Cu in the Cu-CHA catalysts and thus determines the SCR activity[4, 9, 11-13]. Paolucci et al.[9] showed that Cu ions can be assigned to two distinct types based on their proximity to one or two framework Al within a six or eight-membered rings, forming single framework-coordinated 1AlCu or double framework-coordinated 2AlCu sites. The ratio between 1AlCu and 2AlCu sites is dependent on the Si/Al and Cu/Al ratios in Cu-CHA zeolite. A Cu compositional phase diagram has been previously calculated. According to this diagram, catalysts dominated by 1AlCu site show considerably better performance than the catalysts dominated by 2AlCu sites in kinetics studies,[4] suggesting differences in the catalytic mechanism. Furthermore, recent FTIR and temperature programmed desorption studies found that $Cu^{II}NO_x$ only forms on the 1AlCu sites[12,13]. The understanding of different oxidation mechanisms at 1AlCu and 2AlCu sites is therefore important to guide the catalyst design for low temperature SCR and thereby better catalysts.

Here we identify that side-on coordination of O_2 on a $Cu^I(NH_3)_xO_{fw}$ (O_{fw}=framework O from zeolite) intermediate[14] is the rate limiting step in the oxidation half cycle in the nitrate mechanism. The oxidation of Cu^I can only occur when Cu is not directly coordinated to framework oxygen species (O_{fw}). The release of Cu from the framework is site dependent and is thermodynamically hindered when Cu is in proximity to 2Al ions, preventing the transient $Cu^{II}NO_x$ formation, and the release of N_2. As a result, 2AlCu will mainly proceed with the dimer mechanism whereas 1AlCu favors nitrate mechanism. This discovery is based on the combination of *Operando* X-ray Absorption Fine Structure (XAFS), valence to core - X-ray emission spectroscopy (VtC-XES) and density functional theory (DFT) calculations,

demonstrating Cu speciation, changes between Cu-N and Cu-O coordination, and a much stronger Cu-O_{fw} interaction in 2AlCu (67 kJ·mol^{-1}) compared to 1AlCu (28 kJ·mol^{-1}). This result provides a complementary route towards the widely accepted Cu dimer mechanism[10, 15] for splitting O-O at low temperature, bringing new insight towards an atomic level understanding of the complex SCR mechanism.

2. Materials and Method

2.1 Sample Preparation

Pure CHA zeolite and two Cu-CHA samples representing 1AlCu (3 wt% Cu SAR25) and 2AlCu (1 wt% Cu SAR13) were provided by Johnson Matthey Technology Centre in the form of powder. The sample with 1 wt% Cu SAR25 is synthesized with the pure zeolite provided through impregnation. The actual loadings of Cu-CHA samples were verified by ICP-MS analysis.

2.2 Time-resolved XAS and EXAFS

The measurement is carried out in the P64 beamline at Deutsches Elektronen Synchrotron (DESY, Germany). The time-resolved spectra were recorded in fluorescence mode with Si(111) double crystal monochromator. In the experiment 1 wt% Cu SAR25 sample is loaded in the 0.5 mm diameter quartz capillary tube. The same gas configuration with the HERFD-XANES experiments was used and monitored with mass spectrometer. The dynamic spectra (time resolution 60s/spectrum) were recorded between 8780-9380 eV in fluorescence mode with Si(111) double crystal monochromator. XANES and EXAFS under static conditions of each gas

composition were also recorded between 8780-9980 eV in fluorescence mode. The sample was first fully reduced under NH_3+NO and equilibrated for at least 30 min. The gas flow was then switched to NO+O_2 or O_2 when the time series of XAS spectra were initialized. The spectra were recorded every 60 seconds while the catalytic activity was simultaneously monitored by online mass spectrometer connected to the outlet of *in situ* tube. The spectra processing and LCF analysis were also performed with Athena, and EXAFS fitting was performed using Artemis[16].

2.3 HERFD-XANES and XES

HERFD-XANES and non-resonant XES measurements were carried out in the I20-Scanning beamline[17] at Diamond Light Source (DLS, UK). The incident beam energy was selected using a Si(111) 4-bounce scanning monochromator[18]. The X-ray emission spectrometer equipped with three Si(642) spherical analyzers, operated in the Johann configuration with a 1 m diameter Rowland circle[19]. For the *in-situ* measurement, Cu-CHA powders were fixed inside the 3mm diameter Kapton and quartz tubes to be measured under lower temperature (200 ºC) and higher temperature (400 ºC) respectively. The temperature is controlled by a thermocouple inserted into the catalytic bed. Operando experiments were carried out by flowing a constant SCR-related gas mixture (20 mL·min^{-1} with concentration 1000 ppm NO, 1000 ppm NH_3, 10% O_2, balancing He) generated by mass flow controllers. The concentration of the respective gas was kept the same with balancing He while changing the composition of gas flow, which was monitored through mass spectrometer connected to the outlet. The 1AlCu and 2AlCu catalysts are studied under conditions aimed to represent the steady states of the SCR cycle: fully oxidised form under O_2, followed by reduction under NH_3 or NO+NH_3 until the fully reduced catalyst is obtained, and reoxidation under NH_3+O_2, NO+O_2 and NH_3+NO_2+O_2 gas streams. The sequence of different

atmospheres follows the order O_2, NO, NH_3, NO+NH_3, NO+O_2, NH_3+O_2, SCR condition (NO+NH_3+O_2) to avoid interference. The spectra measurement always started after the stabilization of gas flow. Under each condition, $K\beta_{1,3}$ XES (3p□1s) and several HERFD-XANES spectra were recorded until the catalysts reached stable states before the measurement of vtc-XES. HERFD-XANES spectra were also recorded after vtc-XES to check the radiation damage. For the *ex-situ* measurement, pellets were made for $Cu(OH)_2$ and $Cu(NO_3)_2{\cdot}3H_2O$ references with 13 mm die under 3-5 tons pressure for 1-1.5 min. Liquid references ($CuSO_4$ and $[Cu(NH_3)_4]SO_4$ solution) were loaded inside a liquid cell (1.5 mm thickness) sealed with Kapton tapes. High/low concentration samples were made separately to be used for vtc-XES and HERFD-XANES to avoid self-absorption.

HERFD-XANES was measured at the peak of the $K\beta_{1,3}$ emission line between 8903.9 and 8905.3 eV, while scanning the incident energy between 8800-9400 eV with region-scan mode (edge region step = 0.3 eV). The spectra merging, background subtraction, normalization and LCF analysis were performed with Athena[16]. The R-factor for LCF is generally below 0.01, except for NH_3-coordinated conditions under 400 ºC (R-factor > 0.05). The main edge peak is determined by the smallest second-derivative of the spectra. Fixing the excitation energy at 9400 eV, $K\beta_{1,3}$ XES was measured between 8890-8920 eV with 0.3 eV step, and VtC-XES was measured between 8930-9020 eV with region-scan mode ($K\beta_{2,5}$ peak region step = 0.3 eV). Three repetitions (~40 min) were taken under each condition, making total measurement time of 2 hours for each VtC-XES. Three spectra were merged, and the background was subtracted by fitting $K\beta_{1,3}$ emission line with Voigt functions. The VtC XES spectra are normalized to the intensity of $K\beta_{1,3}$ in order to compare the emission for different samples and under different temperatures.

2.4 Computational Details

Density functional theory (DFT) calculations were performed using the CRYSTAL17 code and the PBE0 hybrid exchange functional[20]. The crystalline orbitals are treated as a linear combination of atomic orbitals, represented as a linear combination of Gaussian functions. All-electron basis sets of at least double-zeta plus polarization quality were used for all atoms, obtained from the CRYSTAL online library (www.crystal.unito.it/basis-sets.php) with codes: H_3-1p1G_gatti_1994, O_6-31d1_gatti_1994, Al_85-11G*_gatti_1994, Si_civalleri_1998, Cu_86-4111(41D)G_doll_2000, N_6-31d1G_gatti_1994. Reciprocal space integration has been performed using a 2x2x2 Monkhorst-Pack grid, which gives 8 k points in the irreducible Brillouin zone. Default values were used as convergence criteria for the geometry optimizations and activation barrier calculations. All calculations employ the hexagonal SSZ-13 unit cell with 108 framework atoms plus the Cu complex and gas phase molecules, in P1 space group. Activation barriers are calculated using the distinguished reaction coordinate method, corresponding to a series of constrained geometry optimisations in which a distance (N-O or O-O) representing each elementary reaction step is held constant at regular intervals between its value in reagents and products. The reaction profile corresponds to the variation of calculated energy as a function of the chosen reaction coordinate. Steps of ~0.1 Å or less have been used in the proximity of each transition state.

3. Results and Discussion

3.1 Formation of transient $Cu^{I}(NH_3)_xO_{fw}$ and $Cu^{II}NO_x$ intermediate

The oxidation half cycle can be studied by switching from reduction half cycle NO + NH_3 atmosphere to different oxidation half cycles NO + O_2 or pure O_2. The comparison between these two oxidation conditions can determine the role of NO in the $Cu^{II}NO_x$ mechanism. A model Cu-CHA catalyst with 1 wt% Cu and common Silica: Alumina ratio (SAR25) (~Cu/Al = 0.131) is studied with time-resolved *in situ* XAFS. According to the aforementioned phase diagram,[9] it contains a balanced ratio of 1AlCu and 2AlCu sites and delivers > 95% NO conversion between 225 and 450 ºC (Figure S1). For compelete SCR reaction, the re-oxdation of $Cu^{I}(NH_3)_2$ is hindered by NH3, the $Cu^{II}(NH_3)_4$ can be formed at low temperature. For high temperature, the dominant Cu species are fremework coordinated Cu^{II} sites, forming ZCuOH at 1AlCu site and Z2Cu at 2AlCu. When the SCR reaction is splited to redction and oxidation part, more detailed Cu speciation change can be observed. In our designed experiment, the sample is pre-oxidized in O2 at 400 °C, and reduce to 200 °C. Then the sample is completely reduced to Cu^{I} under NO + NH_3 as shown in the typical $Cu^{I}(NH_3)_2$ 1s $\rightarrow$ 4p X-ray Absorption Near-Edge Structure (XANES) feature at the Cu K-edge 8983 eV (Figure 1a, top red). Changing to NO + O_2 at 200 °C, the $Cu^{I}(NH_3)_2$ feature at 8983 eV disappears along with an increase in the white-line intensity at 8996 eV (Figure 1a, top black), indicating oxidation to Cu^{II}. The decrease of $Cu^{I}(NH_3)_2$ feature undergoes two stages (Figure 1a, 200-12000 s and 1200-1800 s). The intermediate state retains ~65% of the initial intensity at 8983 eV, suggesting a majority of Cu^{I} (Figure 1a, top blue). The slight increase of 1s to 4p feature between 400 and 1200 s is due to the release of NH_3 from zeolite framework, creating local reductive environment that forms small amount of Cu^{I} (Figure 1a, right). This is also confirmed in the mass spectrometry data, which

only shows the presence of the NO on the second stage of oxidation (Figure S3e,f). Linear combination fitting (LCF) with a set of reference Cu environments (Figure S2) is carried out to study the Cu speciation during the two-stage oxidation. The LCF result suggests the possible spectroscopic feature of the intermediate Cu sites (See LCF discussion in Supporting

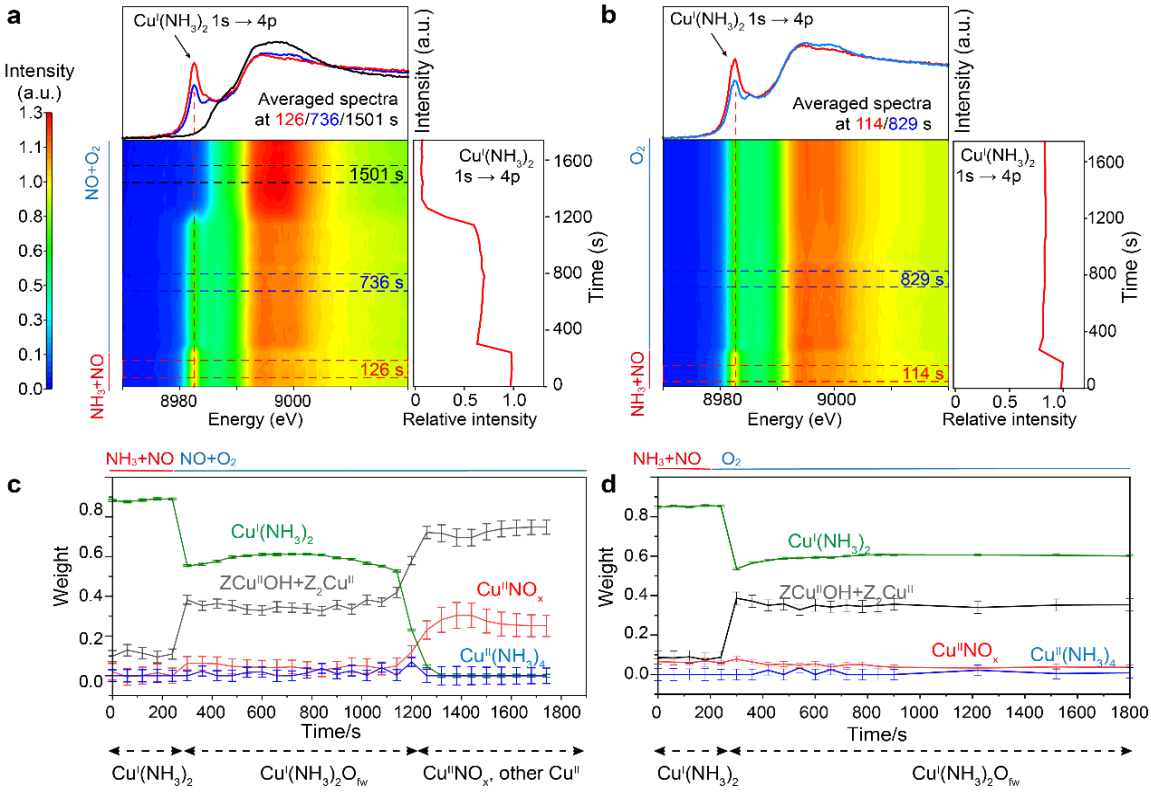

information). The intermediate contains both $Cu^{I}(NH_3)_2$ (Figure 1c green) and Cu-O_{fw} features (Figure 1c black), suggesting a transition from mobile $Cu^{I}(NH_3)_2$ to framework O bonded Cu. Similar behaviour was observed at 400ºC, but with shorter intermediate stage (780 s Vs. 900 s) (Figure S3a and discussion of Cu^{I} oxidation at different temperatures). Transient $Cu^{II}NO_x$ is observed in the second oxidation stage (Figure 1c red), and converts partially to framework coordinated Cu^{II} (Figure 1c blue, black, Figure S4b). Such $Cu^{II}NO_x$ can be immediately reduced to Cu^{I} upon switching to the reductive NO + NH_3 environment, suggesting that it is an important intermediate species during oxidation half cycle.

Figure 1. Time-resolved XAS transient experiments. a,b) XANES spectra heatmap and c,d) Cu speciation during the transient experiments of 1 wt% Cu-CHA (SAR25) through Cu oxidation at 200 °C with the mixture of $NO+O_2$ (a, c) or O_2 alone (b, d) after full reduction with $NO+NH_3$. a,b) top Averaged XANES spectra at selected time points. a,b) right Signal intensity of Cu^I 1s-4p transition peak at 8983 eV. The coexistence of $Cu^I(NH_3)_2$ and $ZCu^{II}OH+Z_2Cu^{II}$ in the intermediate stage suggests the formation of $Cu^I(NH_3)_xO_{fw}$.

The oxidation in O2 alone takes much longer than in NO+O2 and remains at the framework-bonded CuI intermediate for reaction at both 200 °C and 400 °C (Figure 1b,d and Figure S3b, 4b). The formation of $Cu^{II}NOx$ is hardly seen due to the lack of NO supply. Only after 2 hours can the CuI species be fully oxidized to Cu^{II} under O2 (Figure S4d).[21] The coordination numbers (C.N.) of Cu species are studied by fitting of Extended XAFS (EXAFS) at initial, intermediate and final stages under NO + O2 oxidation reveals the Cu-N(O) coordination numbers (C.N.) as 2.5 ± 0.2, 3.1 ± 0.3 and 3.2 ± 0.4 respectively at 200 °C; 2.1 ± 0.2, 2.7 ± 0.3 and 3.3 ± 0.5 respectively at 400 °C (Figure S5 and Table S1). The increased C.N. from 2.5 at $Cu^I(NH_3)_2$ to 3.1 at intermediate state is due to the additional Cu-O_{fw} coordination. Following XANES and EXAFS results we refer to this intermediate as $Cu^I(NH_3)_xO_{fw}$ ($1 < x < 2$). The different behaviour towards oxidation with NO+O2 and O2 alone was also observed with in situ electron paramagnetic resonance (EPR)[22]. This difference shows that though both O2 and NO + O2 will form the long lifetime $Cu^I(NH_3)_xO_{fw}$ intermediate, the oxidation of $Cu^I(NH_3)_xO_{fw}$ to $Cu^{II}NO_x$ is only possible with the presence of NO. Therefore, the activation of $Cu^I(NH_3)_xO_{fw}$ to break the CuI-Ofw bond is the rate-limiting step in oxidation half cycle.

3.2 Formation of Cu-O_{fw} and its reduction at 1AlCu and 2AlCu

Time-resolved XAFS on the model catalyst shows formation of a critical $Cu^{I}(NH_3)_xO_{fw}$ intermediate. According to the site-dependent Cu^{II}NOx mechanism[12, 13], the formation of the $Cu^{I}(NH_3)_xO_{fw}$ and its Cu^{I}-O_{fw} bond breaking at 1AlCu and 2AlCu sites can be different. Therefore, two ideal catalysts: 3 wt% Cu (SAR 25, Cu/Al ~ 0.403) and 1 wt% Cu (SAR 13, Cu/Al ~ 0.072) that represent the 1AlCu and 2AlCu sites, and studied here according to the phase diagram predicted by Paolucci et al.[9] 1AlCu samples has better SCR performance than 2AlCu when normalized by number of Cu atoms in the reactor (Figure S6a). The activation energy E_a are 58.4 and 54.0 kJ·mol^{-1} for 1AlCu and 2AlCu sites samples, respectively (Figure S6a,b), which is in good agreement with literature values with different Cu loadings.[4] They have different EPR response due to the distribution of the Cu sites (Figure S6c and SI Section 2.1). XANES were collected with High-Energy Resolution Fluorescence Detection (HERFD) to reveal additional spectral features (Figure 2a,b). The initial HERFD-XANES of 1AlCu and 2AlCu at room temperature are very similar to the aqueous $Cu(H_2O)_6^{2+}$ solution (Figure S7,8). To study the initial Cu-O_{fw} formation, O_2 is applied at 200 and 400 °C, which reduces the white line intensity at 8996 eV and new features at 8986 / 8983 eV arise, indicating the Cu^{II} dehydration that yields bare Cu^{II} species directly coordinated to O_{fw},(Figure 2a, Figure S9a). The 8986 eV feature is Cu 1s → 4pz transition admixing with O-2p states, referred to 1s → 4pz + LMCT (ligand metal charge transfer) shake-down transition[23]. 1AlCu has broadened feature at 8986 eV, suggesting the Cu is coordinated with two O species that have different O 2p energies that causing the broadening of the shake-down transition, whereas the narrow feature at 2AlCu suggests the same O species. This proves the formation of ZCu^{II}OH site (1 O_{fw} + 1 OH) in the

1AlCu and Z_2Cu^{II} site (2 O_{fw}) in 2AlCu. In addition, the higher intensity around 8983 eV for the 1AlCu sample indicates a more prominent self-reduction[24, 25]. The reduction of framework coordinated $ZCu^{II}OH$ and Z_2Cu^{II} is then studied with NO + NH_3 atmosphere, showing a typical 1s→4p transition at 8983 eV observed for a linear $Cu^{I}(NH_3)_2$ complex[25-27] (Figure 2b). The energy and intensity at the peak maximum of this spectral feature changes as a function of catalyst, temperature and gas composition (Figure 2c). We observe shifts to high energy and low intensity upon 1) decreasing the reducing strength of gas from NO + NH_3 to NH_3 and to NH_3 + O_2; 2) from 200 °C (open) to 400 °C (solid); 3) from 1AlCu (black) to 2AlCu (red). Additional features appeared between 8986-8990 eV at 400 ºC (Figure 2b, Figure S10). This suggests the transition from linear to tetrahedral coordination geometry[25, 26] (Supporting Section 2.2.2) as a result of Cu^{I}-O_{fw} bond formation in the $Cu^{I}(NH_3)_xO_{fw}$ intermediate that is sightly favoured on

2AlCu (Figure 1c). Such $Cu^{I}(NH_3)_xO_{fw}$ species is also seen in the LCF fitting of HERFD-XANES with mixed $[Cu^{I}(NH_3)_2]^+$ and Cu-O_{fw} component (Figure 2f). The Cu-O_{fw} component increases at 2AlCu, suggesting a stronger framework binding than 1AlCu[9, 24, 28]. This is also consistent with the $[Cu^{I}(NH_3)_2]^+$ ratio estimated from the intensity of 1s→4p transition peak fitting (Figure 2c black vs red, Figure S11 and Table S2). From these observations, we conclude that reduction at 2AlCu forms more $Cu^{I}(NH_3)_xO_{fw}$ species than 1AlCu, which will affect their behaviours in oxidation half cycle.

Figure 2. Edge region analysis of HERFD-XANES. HERFD-XANES spectra of 1AlCu and 2AlCu samples at 200 °C and 400 °C in a), O_2 and b), $NO+NH_3$. HERFD-XANES removes the

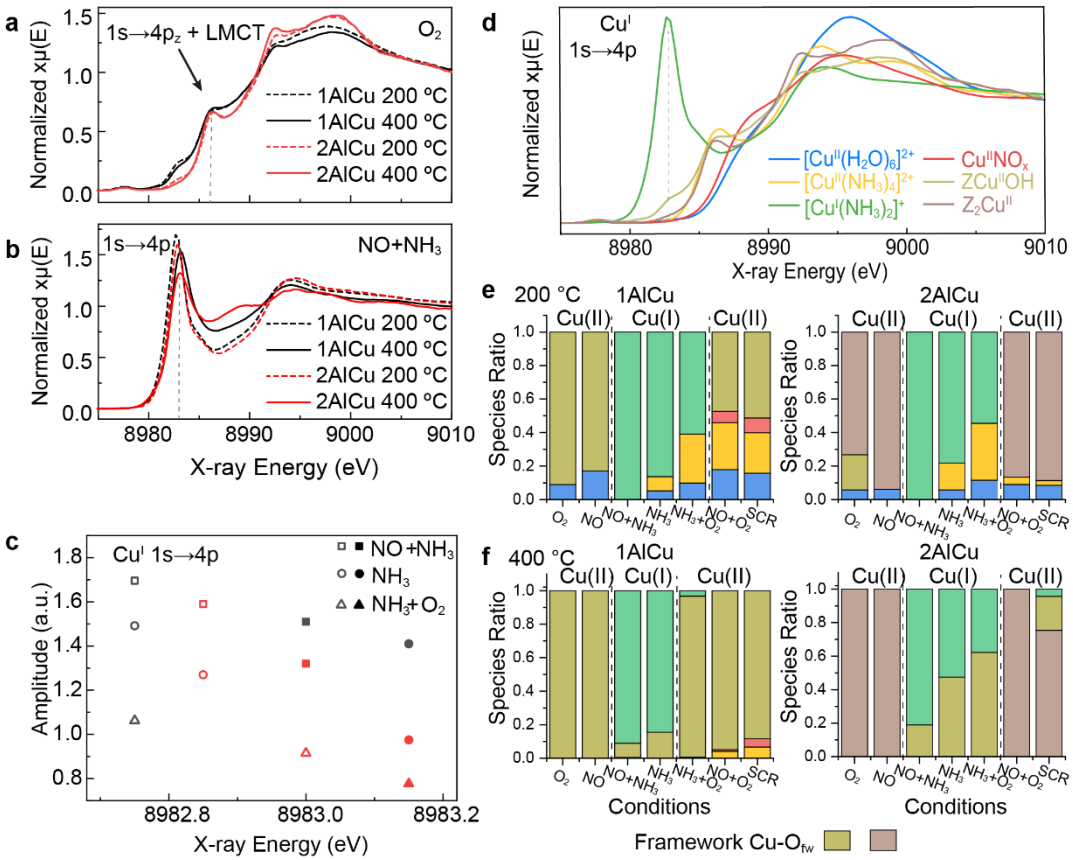

broadening caused by core-hole lifetime and suppress background[29], yielding further information on Cu oxidation state and coordination environment. c) Intensity and energy of the Cu^{I} 1s→4p

transition for Cu-CHA samples under reductive conditions at 200 °C (open) and 400 °C (full symbols): NO+NH_3 (square), NH_3 (circle), NH_3+O_2 (triangle). d) HERFD-XANES spectra of reference compounds used in the LCF. Spectra of Cu-CHA catalysts in O_2 RT and in NO+NH_3 at 200 °C are used as reference for $[Cu^{II}(H_2O)_6]^{2+}$ and $[Cu^{I}(NH_3)_2]^{+}$ in the LCF[8, 27, 30] (Supporting Section 2.2.1). $ZCu^{II}OH$ and Z_2Cu^{II} are represented by spectra collected with 1AlCu and 2AlCu samples at 400 °C in O_2[31, 32]. LCF analysis of Cu speciation in the 1AlCu and 2AlCu samples under different gas conditions at e) 200 °C and f) 400 °C, using the same colour code as in d).

3.3 Oxidation of $Cu^{I}(NH_3)_xO_{fw}$ with formation of $Cu^{II}NO_x$ only at 1AlCu

The 2AlCu catalyst has higher $Cu^{I}(NH_3)_xO_{fw}$ content and stronger binding to O_{fw} than 1AlCu, inhibiting the reoxidation of Cu^{I}. Upon treatment with NH_3 + O_2, the 2AlCu sample yields a mixture of $ZCu^{II}OH$ and $Cu^{I}(NH_3)_xO_{fw}$, while in the 1AlCu sample Cu is completely oxidized to $ZCu^{II}OH$ at 400 °C (Figure 2c,f). Complete Cu^{I} oxidation to Cu^{II} is observed under NO + O_2 at both 200 and 400°C, but with different Cu^{II} speciation in 1AlCu and 2AlCu sites. Co-feeding NO and O_2 into the reduced 1AlCu catalyst yields $Cu^{II}NO_x$ that is not observed with NO or O_2 alone in the gas stream or in 2AlCu (Figure 2e,f). This result indicates that formation of $Cu^{II}NO_x$ (x= 2 or 3) through oxidation of both Cu and NO, only occurs in 1AlCu. $Cu^{II}NO_x$ is also found in time-resolved XAFS (Figure 1c, red). $Cu^{II}NO_x$ is proposed as an important intermediate of the oxidation half cycle[8, 33], further supported here as the $Cu^{II}NO_x$ signal is stronger under SCR condition (NO+NH_3+O_2) than NO+O_2 (Figure 2ef, red), confirming the presence of nitrate species during the catalytic reaction. Even at the fully oxidized state, 2AlCu has high Z_2Cu ratio (Figure 2e), suggesting the stronger Cu-O_{fw} interaction of the latter. As a result, $Cu^{I}(NH_3)_xO_{fw}$ in

1AlCu has weaker Cu-O_{fw} interaction, is easier to oxidize than 2AlCu, forming a $Cu^{II}NO_x$ intermediate and indicating high SCR activity. A higher rate of $Cu^{I}(NH_3)_2$ oxidation is also observed in the 1AlCu sample and will be discussed in a separate publication.

3.4 Evidence of Cu-N bond breaking and Cu-O bond formation

The transition from $Cu^{I}(NH_3)_2$ to $Cu^{I}(NH_3)_xO_{fw}$ and to $Cu^{II}NO_x$ involves a change from Cu-N coordination to mixed Cu-O/N and finally to Cu-O coordination. The change from Cu-N to Cu-O can be studied with VtC-XES[24, 27, 30, 34-36] (Figure 3). VtC spectra are sensitive to the O and N–based ligands[37] because they contain transitions to the Cu 1s core-level from the Cu 3d and 4p valence states that are mixed with ligand 2p ($K\beta_{2,5}$) and 2s orbitals ($K\beta''$ satellite)[35, 38, 39] (Figure 3a). This is not possible with EXAFS fitting. O coordinated $[Cu(H_2O)_6]^{2+}$, $Cu(OH)_2$, $Cu(NO_3)_2{\cdot}3H_2O$ have a double peak $K\beta_{2,5}$ feature at 8972.4/8976.0 eV while N coordinated $[Cu^{II}(NH_3)_4]^{2+}$ has a single peak at 8976.0 eV. In addition, the $K\beta''$ peak shifted from 8951.5 eV in $[Cu(H_2O)_6]^{2+}$ and $Cu(NO_3)_2{\cdot}3H_2O$ to 8955.8 eV in $Cu(OH)_2$ to 8960.0 eV in $[Cu^{II}(NH_3)_4]^{2+}$, indicating the change from H_2O to OH^- and NH_3 ligands. The *operando* VtC XES shows similar features for 1AlCu and 2AlCu samples at 200 ºC (Figure 3c, Figure S13), with $K\beta_{2,5}$ double peak and $K\beta''$ peak position for O-coordination at O_2 / NO + O_2 conditions, and N-coordination in the NH_3 related reductive conditions (Figure 3c green, Figure S13). The red shift of the $K\beta_{2,5}$ single peak from 8976.0 eV in $[Cu(NH_3)_4]^{2+}$ to 8973.6 eV in Cu-CHA suggests reduction to $Cu^{I}(NH_3)_2$[39, 40], consistent with the decrease of the 1s→4p transition energy in XANES (Figure 2a-c). Increasing the temperature to 400 °C does not alter Cu coordination in oxidative conditions (Figure 3d green, Figure S14), however, the double peak feature evolves in reducing conditions

along with the red shift of Kβ'' to 8956.5 eV. This indicates the Cu-O coordination even under NH_3+NO for both 1AlCu and 2AlCu at 400 °C and is the key evidence for the $Cu^{I}(NH_3)_xO_{fw}$ feature observed in HERFD-XANES (Figure 2b,f). The $Cu^{I}(NH_3)_2$ to $Cu^{I}(NH_3)_xO_{fw}$ transformation is observed in changing from NO + NH_3 to NH_3 + O_2. In 1AlCu, the $K\beta_{2,5}$ feature under NH_3+O_2 is very similar to the initial fully oxidised state, indicating the oxidation to $ZCu^{II}OH$ (Figure 3e). The 2AlCu maintains the Cu-N feature at 8973.0 eV, showing a mixture of Cu-N and Cu-O coordination (Figure 3f). Together with HERFD-XANES result, we conclude that 2AlCu contains a mixture of $Cu^{I}(NH_3)_xO_{fw}$ and $Z_2Cu^{II}/ZCu^{II}OH$ species. The complete conversion from $Cu^{I}(NH_3)_xO_{fw}$ to Z_2Cu^{II} and $ZCu^{II}OH$ at 2AlCu requires the simultaneous presence of NO and O_2 for at least 1 hour (Figure S14b). The VtC-XES results confirm the swift Cu-N to Cu-O conversion at 1AlCu but 2AlCu stays with a mixture of Cu-N/O under NH_3 + O_2.

Figure 3. Valence-to-core XES of 1AlCu and 2AlCu samples. a) Simplified molecular orbital

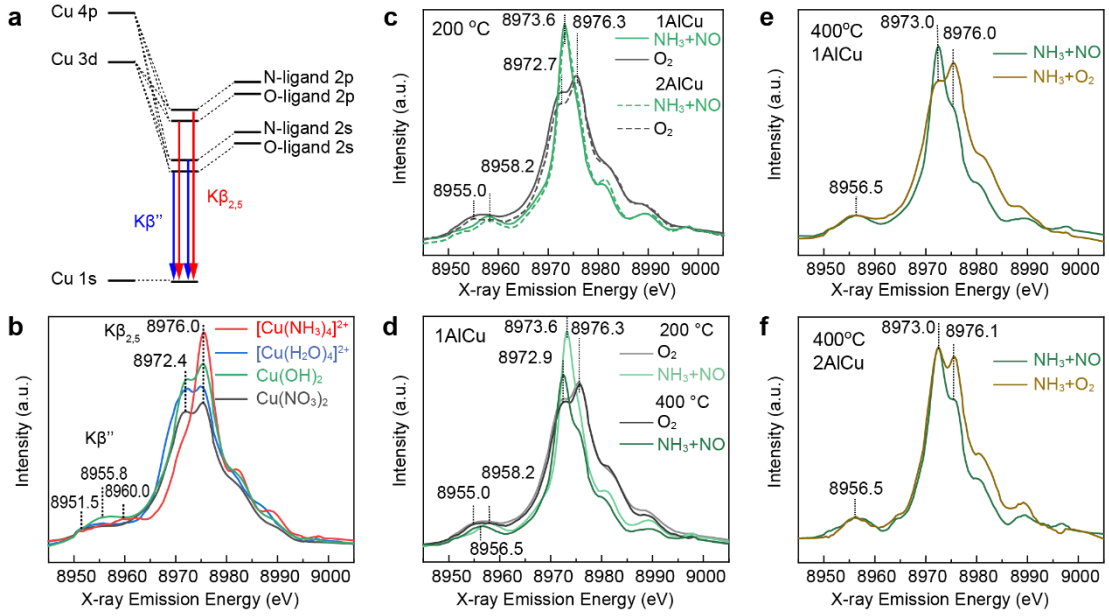

diagram depicting VtC transitions from N-coordinated and O-coordinated complexes. b) Vtc-XES spectra for Cu reference compounds; c) comparison of N-coordination and O-coordination

in 1AlCu and 2AlCu at 200 °C; d) comparison of 1AlCu at 200 °C and 400 °C; VtC spectra in NH_3+NO and NH_3+O_2 for e) 1AlCu and f) 2AlCu at 400 °C.

3.5 Computational analysis

DFT calculations have been performed to examine Cu-O_{fw} binding in 1AlCu and 2AlCu samples and the different activation barriers of Cu^I oxidation towards $Cu^{II}NO_x$ (Supporting, DFT discussion). The adsorption energy of O_2, NO, H_2O, and NH_3 to isolated $Cu^I(NH_3)_2$ is first calculated (Table S4). $Cu^I(NH_3)_2$, as confirmed here with HERFD-XANES (Figure 2b), is the predominant species at the end of the reduction half cycle.[6, 9] O_2 out-binds NO and has two distinct modes of adsorption upon $Cu^I(NH_3)_2$: side-on and end-on (Figure S15). The former adsorbs 46 $kJmol^{-1}$ more strongly than the latter.

DFT results confirm the Cu-O_{fw} interaction observed in XANES and XES: the framework-coordinated $Cu^I(NH_3)_2$ species. Only by increasing the Cu coordination number, such as by adsorption of NO, O_2 or additional NH_3 molecules, can Cu be released from the direct interaction with O_{fw}. When NO and O_2 molecules are co-adsorbed on $Cu^I(NH_3)_2$, the framework-coordinated and free Cu complexes are distinct local minima in the energy surface; in 1AlCu releasing Cu from O_{fw} requires 28 $kJ{\cdot}mol^{-1}$ against 67 $kJ{\cdot}mol^{-1}$ in 2AlCu, a significant difference for the low-temperature SCR. The stronger interaction of Cu^I with the framework in 2AlCu has electrostatic origin, since the Al ion replacing Si in the zeolite represents a lattice defect with negative net charge. This result suggests a shift towards framework-coordinated Cu from mobile Cu, as well as slower Cu-O_{fw} bond-breaking dynamics, in the 2AlCu.

Framework-coordinated Cu invariably yields end-on O_2 adsorption while in absence of Cu-O_{fw} bonds we observe side-on coordination of O_2, for both 1AlCu and 2AlCu sites (Figure 4a). Side-on O_2 enables backdonation of electrons from Cu to the π^* molecular orbital, activating O-O dissociation; this is validated by the equilibrium O-O bond length of 1.33Å compared to 1.22Å for end-on coordination. The release of Cu^I complexes from the framework to enable the activated side-on coordination of O_2 to Cu^I is therefore a critical step in the oxidation half cycle.

Oxidation of $Cu^I(NH_3)_2$ in 1AlCu and 2AlCu environments is then considered with a range of initial coordination environments, varying the type, number and relative orientation of gas phase ligands (Figure S17). Only when NO and O_2 are present simultaneously have we been able to observe a stable product for the Cu^I oxidation, corresponding to formation of nitrate ions:

$$Cu^I(NH_3)_2(NO)(O_2) \rightarrow Cu^{II}(NH_3)_2(NO_3^-)$$

We identified a three-step mechanism (Figure 4b): 1) attack of NO to O_2 to yield a peroxynitrite ion ($ONOO^-$) with simultaneous oxidation of Cu^I to Cu^{II}; 2) O-O bond dissociation to yield O^- and NO_2 both coordinated to Cu^{II}; 3) bond formation between O^- and NO_2 to form NO_3^-.

The formation of NO_3^- does not occur for fw-coordinated Cu in $Cu(NH_3)_xO_{fw}$: even if the $Cu(O_{fw})$-OONO intermediate forms with low barrier (ΔE1 in Fig 4c), subsequent O-O dissociation (ΔE2 in Fig 4c) requires in excess of 140 kJ·mol^{-1}. If however O2 adsorption occurs on released $Cu(NH_3)_2O_2$, leading to side-on coordination, NO addition to O_2 occurs readily, and O-O dissociation requires a reduced activation barrier of 82-83 kJmol^{-1}. The latter is also likely in the SCR condition given the higher O_2 content than NO and O_2 out-binds NO in Cu coordination. Formation of NO_3^- from NO_2^- and O coordinated to Cu (□E3 in Fig 4c) is fast in all cases. The calculated reaction barriers indicate that the oxidation mechanism is similar in

1AlCu and 2AlCu and requires release of Cu from framework coordination to progress. What differentiates 1AlCu and 2AlCu environments is the strength of the Cu-O_{fw} coordination, that makes formation of framework-free Cu much easier in the 1AlCu, in turn activating O_2 for bond dissociation.

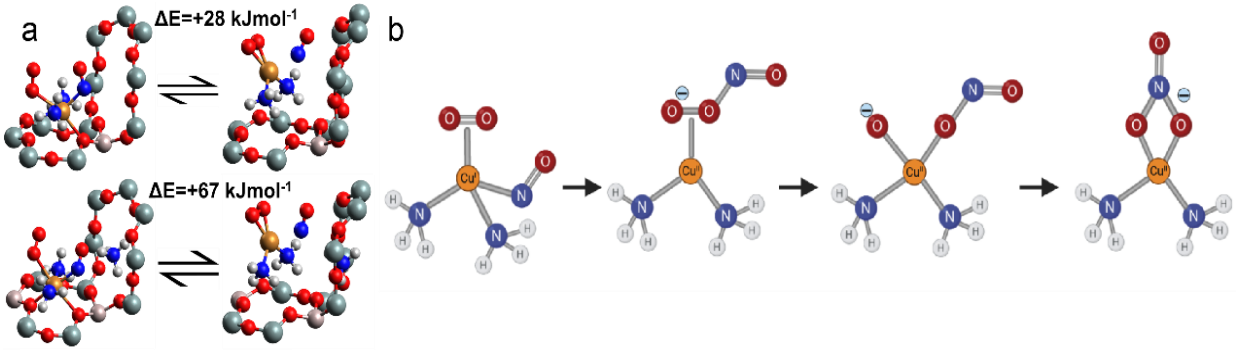

c Site	Coordination Environment	ΔE_1/kJmol^{-1}	ΔE_2/kJmol^{-1}	ΔE_3/kJmol^{-1}
1AlCu	Cu^I-O_{fw}, NO in 2nd SS, end-on O_2	4.9	143	10
	Free Cu^I, co-adsorbed NO, side-on O_2	**27**	**83**	**3.5**
2AlCu	Cu^I-O_{fw}, NO in 2nd SS, end-on O_2	18	140	4
	Free Cu^I, co-adsorbed NO, side-on O_2	**60**	**82**	**36**

Figure 4. a) Equilibrium structures and calculated energy difference between framework coordinated and free Cu^I at 1AlCu (top) and 2AlCu (bottom) sites, described under periodic boundary conditions. For 2AlCu site, an NH_4^+ ion situated in the 8-member ring is used for charge balance and the 2 Al ions are located as the 3rd nearest neighbours in the 6-memberring[8, 9]. b) Elementary reaction steps in the formation of NO_3^- and calculated activation barriers (□E1, □E2, □E3 in kJ mol^{-1}) for the different Cu^I environments considered. c) Table showing the activation barrier for each step in b) at the different coordination environments for 1Al and 2Al sites.

4. Conclusion

A complex reaction, such as SCR in the framework of Cu-CHA, usually undergoes several reaction pathways/mechanisms. The distribution and ratio between those pathways are condition and structure-dependent. The dicopper amino oxygen bridged complexes is a widely accepted intermediate to dissociate the O-O bond in the oxidation half cycle at low temperature. In addition to this mechanism, here we discover a complementary pathway by combining time-resolved XAFS, steady state HERFD-XANES and vtc-XES and DFT analysis (Table S3). Under low temperatures, reduced $Cu^{I}(NH_3)_2$ species formed at the end of the reduction half-cycle yield direct Cu-framework coordination, indicated as $Cu^{I}(NH_3)_xO_{fw}$. The stronger Cu^{I}-O_{fw} binding in 2AlCu means it is significantly harder for Cu to be released from the framework compared to 1AlCu sites. Steric crowding around Cu caused by the Cu-O_{fw} interactions leads to unreactive end-on O_2 coordination; activated side-on O_2 coordination is instead observed when Cu is freed from the framework. This geometry facilitates the formation of nitrate intermediates, in which Cu(I) and NO are simultaneously oxidised by O_2; the oxidation happens preferentially on 1AlCu sites in which a higher fraction of Cu is released from the framework. The sequence of species in the oxidation process follows $Cu^{I}(NH_3)_2 \rightarrow Cu^{I}(NH_3)_xO_{fw} \rightarrow Cu^{I}(NH_3)_x(NO)(O_2)Cu^{I}(NH_3)_x(OONO) \rightarrow Cu^{II}(NH_3)_x(NO_3) \rightarrow$ Z-Cu^{II} ($ZCu^{II}OH+Z_2Cu^{II}$) (Figure 4). The result provides an additional mechanistic route for the oxidation half cycle, complementary to the proposed dimer mechanism[41]. It shows that side-on O_2 is a proper intermediate configuration to split O-O at 1AlCu site. Changing the Cu site geometry may proceed the O-O split in different ways, as shown here in the nitrate mechanism and the common dimer mechanism. Together with the existing literature, the study here provides a complete understanding to the SCR mechanism. At low Cu loadings and low temperature (< 250 °C) SCR proceeds with dimer mechanism. At high Cu loadings and low temperature (< 250 °C), the

reaction combines dimer, nitrate and also CuO cluster mechanisms to split O-O bond. At high temperature (> 250 °C), the Cu species is not mobile and rules out the dimer mechanism. Therefore, understanding of coordination chemistry and catalysis in such confined environment is critical for rational design and optimisation of new catalytic reactions with high activity and selectivity.

Data availability

Additional data can be found in the Supporting Information (Figure S1–19, Tables S1–5 and related discussions). The data that support the findings of this study are available from the corresponding authors Furio Cora. (email: f.cora@ucl.ac.uk) or Feng Ryan Wang. (email: ryan.wang@ucl.ac.uk) upon reasonable request.

Acknowledgements

We acknowledge the funding support EPSRC (EP/P02467X/1 and EP/S018204/2), Royal Society (RG160661, IES\R3\170097, IES\R1\191035 and IEC\R3\193038), the Newton International Fellowship (NF170761) and the UCL-Johnson Matthey impact studentship. We acknowledge the Johnson Matthey Technology Centre for providing the catalysts. We acknowledge the Diamond Light Source for the HERDF-XANES and vtc-XES experiments beamtime at I20-scanning beamline (SP24285) and the beamline scientists for the provision of beamtime. We acknowledge the Deutsches Elektronen-Synchrotron (DESY), a member of the Helmholtz Association (HGF), for the XAFS beamtime at beamline P64 in PETRA III (I-20190358) and the beamline scientists for the provision of the beamtime. We acknowledge the Chinese Scholarship Council for the studentship of Yiyun Liu.

Reference

1. Beale, A. M.; Gao, F.; Lezcano-Gonzalez, I.; Peden, C. H.; Szanyi, J., Recent advances in automotive catalysis for NOx emission control by small-pore microporous materials. *Chemical Society Reviews* **2015,** *44* (20), 7371-7405.
2. Borfecchia, E.; Beato, P.; Svelle, S.; Olsbye, U.; Lamberti, C.; Bordiga, S., Cu-CHA - a model system for applied selective redox catalysis. *Chemical Society Reviews* **2018,** *47* (22), 8097-8133.
3. Gao, F.; Kwak, J. H.; Szanyi, J.; Peden, C. H., Current understanding of Cu-exchanged chabazite molecular sieves for use as commercial diesel engine DeNOx catalysts. *Topics in Catalysis* **2013,** *56* (15-17), 1441-1459.
4. Gao, F.; Washton, N. M.; Wang, Y.; Kollár, M.; Szanyi, J.; Peden, C. H., Effects of Si/Al ratio on Cu/SSZ-13 NH_3-SCR catalysts: Implications for the active Cu species and the roles of Brønsted acidity. *Journal of Catalysis* **2015,** *331*, 25-38.
5. Kwak, J. H.; Lee, J. H.; Burton, S. D.; Lipton, A. S.; Peden, C. H.; Szanyi, J., A Common Intermediate for N_4 Formation in Enzymes and Zeolites: Side‐On Cu–Nitrosyl Complexes. *Angewandte Chemie International Edition* **2013,** *52* (38), 9985-9989.
6. Gao, F.; Mei, D. H.; Wang, Y. L.; Szanyi, J.; Peden, C. H. F., Selective Catalytic Reduction over Cu/SSZ-13: Linking Homo- and Heterogeneous Catalysis. *J Am Chem Soc* **2017,** *139* (13), 4935-4942.
7. Paolucci, C.; Verma, A. A.; Bates, S. A.; Kispersky, V. F.; Miller, J. T.; Gounder, R.; Delgass, W. N.; Ribeiro, F. H.; Schneider, W. F., Isolation of the copper redox steps in the standard selective catalytic reduction on Cu-SSZ-13. *Angew Chem Int Ed Engl* **2014,** *53* (44), 11828-33.
8. Janssens, T. V. W.; Falsig, H.; Lundegaard, L. F.; Vennestrom, P. N. R.; Rasmussen, S. B.; Moses, P. G.; Giordanino, F.; Borfecchia, E.; Lomachenko, K. A.; Lamberti, C.; Bordiga, S.; Godiksen, A.; Mossin, S.; Beato, P., A Consistent Reaction Scheme for the Selective Catalytic Reduction of Nitrogen Oxides with Ammonia. *Acs Catal* **2015,** *5* (5), 2832-2845.
9. Paolucci, C.; Parekh, A. A.; Khurana, I.; Di Iorio, J. R.; Li, H.; Caballero, J. D. A.; Shih, A. J.; Anggara, T.; Delgass, W. N.; Miller, J. T.; Ribeiro, F. H.; Gounder, R.; Schneider, W. F., Catalysis in a Cage: Condition-Dependent Speciation and Dynamics of Exchanged Cu Cations in SSZ-13 Zeolites. *J Am Chem Soc* **2016,** *138* (18), 6028-6048.
10. Paolucci, C.; Khurana, I.; Parekh, A. A.; Li, S. C.; Shih, A. J.; Li, H.; Di Iorio, J. R.; Albarracin-Caballero, J. D.; Yezerets, A.; Miller, J. T.; Delgass, W. N.; Ribeiro, F. H.; Schneider, W. F.; Gounder, R., Dynamic multinuclear sites formed by mobilized copper ions in NOx selective catalytic reduction. *Science* **2017,** *357* (6354), 898-903.
11. Song, J.; Wang, Y.; Walter, E. D.; Washton, N. M.; Mei, D.; Kovarik, L.; Engelhard, M. H.; Prodinger, S.; Wang, Y.; Peden, C. H., Toward rational design of Cu/SSZ-13 selective catalytic reduction catalysts: Implications from atomic-level understanding of hydrothermal stability. *Acs Catal* **2017,** *7* (12), 8214-8227.
12. Villamaina, R.; Liu, S. J.; Nova, I.; Tronconi, E.; Ruggeri, M. P.; Collier, J.; York, A.; Thompsett, D., Speciation of Cu Cations in Cu-CHA Catalysts for NH3-SCR: Effects of SiO2/AlO3 Ratio and Cu-Loading Investigated by Transient Response Methods. *Acs Catal* **2019,** *9* (10), 8916-8927.

13. Negri, C.; Hammershoi, P. S.; Janssens, T. V. W.; Beato, P.; Berlier, G.; Bordiga, S., Investigating the Low Temperature Formation of Cu-II-(N,O) Species on Cu-CHA Zeolites for the Selective Catalytic Reduction of NOx. *Chem.-Eur. J.* **2018,** *24* (46), 12044-12053.
14. Borfecchia, E.; Negri, C.; Lomachenko, K. A.; Lamberti, C.; Janssens, T. V. W.; Berlier, G., Temperature-dependent dynamics of $NH3_3$-derived Cu species in the Cu-CHA SCR catalyst. *Reaction Chemistry & Engineering* **2019,** *4* (6), 1067-1080.
15. Negri, C.; Selleri, T.; Borfecchia, E.; Martini, A.; Lomachenko, K. A.; Janssens, T. V. W.; Cutini, M.; Bordiga, S.; Berlier, G., Structure and Reactivity of Oxygen-Bridged Diamino Dicopper(II) Complexes in Cu-Ion-Exchanged Chabazite Catalyst for NH_3-Mediated Selective Catalytic Reduction. *J Am Chem Soc* **2020,** *142* (37), 15884-15896.
16. Ravel, B.; Newville, M., ATHENA, ARTEMIS, HEPHAESTUS: data analysis for X-ray absorption spectroscopy using IFEFFIT. *Journal of Synchrotron Radiation* **2005,** *12* (4), 537-541.
17. Diaz-Moreno, S.; Amboage, M.; Basham, M.; Boada, R.; Bricknell, N. E.; Cibin, G.; Cobb, T. M.; Filik, J.; Freeman, A.; Geraki, K.; Gianolio, D.; Hayama, S.; Ignatyev, K.; Keenan, L.; Mikulska, I.; Mosselmans, J. F. W.; Mudd, J. J.; Parry, S. A., The Spectroscopy Village at Diamond Light Source. *J Synchrotron Radiat* **2018,** *25* (Pt 4), 998-1009.
18. Hayama, S.; Duller, G.; Sutter, J. P.; Amboage, M.; Boada, R.; Freeman, A.; Keenan, L.; Nutter, B.; Cahill, L.; Leicester, P.; Kemp, B.; Rubies, N.; Diaz-Moreno, S., The scanning four-bounce monochromator for beamline I20 at the Diamond Light Source. *Journal of Synchrotron Radiation* **2018,** *25* (5), 1556-1564.
19. Hayama, S.; Boada, R.; Chaboy, J.; Birt, A.; Duller, G.; Cahill, L.; Freeman, A.; Amboage, M.; Keenan, L.; Diaz-Moreno, S., Photon-in/photon-out spectroscopy at the I20-scanning beamline at diamond light source. *Journal of Physics: Condensed Matter* **2021,** *33* (28), 284003.
20. Dovesi, R.; Orlando, R.; Erba, A.; Zicovich‐Wilson, C. M.; Civalleri, B.; Casassa, S.; Maschio, L.; Ferrabone, M.; De La Pierre, M.; d'Arco, P., CRYSTAL14: A program for the ab initio investigation of crystalline solids. *International Journal of Quantum Chemistry* **2014,** *114* (19), 1287-1317.
21. Daya, R.; Trandal, D.; Menon, U.; Deka, D. J.; Partridge, W. P.; Joshi, S. Y., Kinetic Model for the Reduction of Cu(II)Sites by NO + NH(3)and Reoxidation of NH3-Solvated Cu(I)Sites by O(2)and NO in Cu-SSZ-13. *Acs Catalysis* **2022,** *12* (11), 6418-6433.
22. Godiksen, A.; Isaksen, O. L.; Rasmussen, S. B.; Vennestrom, P. N. R.; Mossin, S., Site-Specific Reactivity of Copper Chabazite Zeolites with Nitric Oxide, Ammonia, and Oxygen. *Chemcatchem* **2018,** *10* (2), 366-370.
23. Hocking, R. K.; Solomon, E. I., Ligand Field and Molecular Orbital Theories of Transition Metal X-ray Absorption Edge Transitions. **2011,** *142*, 155-184.
24. Borfecchia, E.; Lomachenko, K. A.; Giordanino, F.; Falsig, H.; Beato, P.; Soldatov, A. V.; Bordiga, S.; Lamberti, C., Revisiting the nature of Cu sites in the activated Cu-SSZ-13 catalyst for SCR reaction. *Chemical Science* **2015,** *6* (1), 548-563.
25. Rudolph, J.; Jacob, C. R., Revisiting the Dependence of Cu K-Edge X-ray Absorption Spectra on Oxidation State and Coordination Environment. *Inorg Chem* **2018,** *57* (17), 10591-10607.
26. Kau, L. S.; Spira-Solomon, D. J.; Penner-Hahn, J. E.; Hodgson, K. O.; Solomon, E. I., X-ray absorption edge determination of the oxidation state and coordination number of copper.

Application to the type 3 site in Rhus vernicifera laccase and its reaction with oxygen. *J Am Chem Soc* **1987,** *109* (21), 6433-6442.
27. Lomachenko, K. A.; Borfecchia, E.; Negri, C.; Berlier, G.; Lamberti, C.; Beato, P.; Falsig, H.; Bordiga, S., The Cu-CHA deNO(x) Catalyst in Action: Temperature-Dependent NH_3-Assisted Selective Catalytic Reduction Monitored by Operando XAS and XES. *J Am Chem Soc* **2016,** *138* (37), 12025-12028.
28. Andersen, C. W.; Borfecchia, E.; Bremholm, M.; Jørgensen, M. R. V.; Vennestrøm, P. N. R.; Lamberti, C.; Lundegaard, L. F.; Iversen, B. B., Redox‐Driven Migration of Copper Ions in the Cu‐CHA Zeolite as Shown by the In Situ PXRD/XANES Technique. *Angewandte Chemie International Edition* **2017,** *56* (35), 10367-10372.
29. Hämäläinen, K.; Siddons, D. P.; Hastings, J. B.; Berman, L. E., Elimination of the inner-shell lifetime broadening in x-ray-absorption spectroscopy. *Physical Review Letters* **1991,** *67* (20), 2850-2853.
30. Giordanino, F.; Borfecchia, E.; Lomachenko, K. A.; Lazzarini, A.; Agostini, G.; Gallo, E.; Soldatov, A. V.; Beato, P.; Bordiga, S.; Lamberti, C., Interaction of NH3 with Cu-SSZ-13 catalyst: a complementary FTIR, XANES, and XES study. *The journal of physical chemistry letters* **2014,** *5* (9), 1552-1559.
31. Martini, A.; Borfecchia, E.; Lomachenko, K. A.; Pankin, I. A.; Negri, C.; Berlier, G.; Beato, P.; Falsig, H.; Bordiga, S.; Lamberti, C., Composition-driven Cu-speciation and reducibility in Cu-CHA zeolite catalysts: a multivariate XAS/FTIR approach to complexity. *Chemical Science* **2017,** *8* (10), 6836-6851.
32. Marberger, A.; Petrov, A. W.; Steiger, P.; Elsener, M.; Kröcher, O.; Nachtegaal, M.; Ferri, D., Time-resolved copper speciation during selective catalytic reduction of NO on Cu-SSZ-13. *Nature Catalysis* **2018,** *1* (3), 221-227.
33. Greenaway, A. G.; Marberger, A.; Thetford, A.; Lezcano-González, I.; Agote-Arán, M.; Nachtegaal, M.; Ferri, D.; Kröcher, O.; Catlow, C. R. A.; Beale, A. M., Detection of key transient Cu intermediates in SSZ-13 during NH_3-SCR deNOx by modulation excitation IR spectroscopy. *Chemical Science* **2020,** *11* (2), 447-455.
34. Bergmann, U.; Glatzel, P., X-ray emission spectroscopy. *Photosynth Res* **2009,** *102* (2-3), 255-66.
35. Glatzel, P.; Bergmann, U., High resolution 1s core hole X-ray spectroscopy in 3d transition metal complexes—electronic and structural information. *Coordination Chemistry Reviews* **2005,** *249* (1), 65-95.
36. Günter, T.; Carvalho, H. W. P.; Doronkin, D. E.; Sheppard, T.; Glatzel, P.; Atkins, A. J.; Rudolph, J.; Jacob, C. R.; Casapu, M.; Grunwaldt, J.-D., Structural snapshots of the SCR reaction mechanism on Cu-SSZ-13. *Chemical Communications* **2015,** *51* (44), 9227-9230.
37. Lim, H.; Baker, M. L.; Cowley, R. E.; Kim, S.; Bhadra, M.; Siegler, M. A.; Kroll, T.; Sokaras, D.; Weng, T. C.; Biswas, D. R.; Dooley, D. M.; Karlin, K. D.; Hedman, B.; Hodgson, K. O.; Solomon, E. I., Kβ X-ray Emission Spectroscopy as a Probe of Cu(I) Sites: Application to the Cu(I) Site in Preprocessed Galactose Oxidase. *Inorg Chem* **2020,** *59* (22), 16567-16581.
38. Bergmann, U.; Bendix, J.; Glatzel, P.; Gray, H. B.; Cramer, S. P., Anisotropic valence →core x-ray fluorescence from a $[Rh(en)_3][Mn(N)(CN)_5]\cdot H_2O$ single crystal: Experimental results and density functional calculations. *The Journal of Chemical Physics* **2002,** *116* (5), 2011-2015.

39. Bergmann, U.; Horne, C. R.; Collins, T. J.; Workman, J. M.; Cramer, S. P., Chemical dependence of interatomic X-ray transition energies and intensities – a study of Mn Kβ″ and $K\beta 2_{2,5}$ spectra. *Chemical Physics Letters* **1999,** *302* (1), 119-124.
40. Lee, N.; Petrenko, T.; Bergmann, U.; Neese, F.; DeBeer, S., Probing Valence Orbital Composition with Iron Kβ X-ray Emission Spectroscopy. *J Am Chem Soc* **2010,** *132* (28), 9715-9727.
41. Chen, L.; Falsig, H.; Janssens, T. V. W.; Gronbeck, H., Activation of oxygen on $(NH_3\text{-}Cu\text{-}NH_3)^+$ in NH_3-SCR over Cu-CHA. *Journal of Catalysis* **2018,** *358*, 179-186.